

Geophysical Research Letters

RESEARCH LETTER

10.1002/2016GL069350

Key Points:

- Relativistic butterfly PADs occur with the highest occurrence rate ~ 80% at ~ 20–04 MLT and $L > \sim 5.5$
- Relativistic butterfly PADs are found to extend to $L = 3.5$ with the rate < 25% and can peak at pitch angles down to ~30°
- Compared to the strong L shell and MLT dependence, relativistic butterfly PADs show much less sensitivity to P_{dyn} , AE*, and energy

Supporting Information:

- Supporting Information S1
- Figure S1
- Figure S2
- Figure S3

Correspondence to:

B. Ni,
bbni@whu.edu.cn

Citation:

Ni, B., Z. Zou, X. Li, J. Bortnik, L. Xie, and X. Gu (2016), Occurrence characteristics of outer zone relativistic electron butterfly distribution: A survey of Van Allen Probes REPT measurements, *Geophys. Res. Lett.*, 43, 5644–5652, doi:10.1002/2016GL069350.

Received 2 MAY 2016

Accepted 23 MAY 2016

Accepted article online 25 MAY 2016

Published online 11 JUN 2016

Occurrence characteristics of outer zone relativistic electron butterfly distribution: A survey of Van Allen Probes REPT measurements

Binbin Ni¹, Zhengyang Zou¹, Xinlin Li², Jacob Bortnik³, Lun Xie⁴, and Xudong Gu¹

¹Department of Space Physics, School of Electronic Information, Wuhan University, Wuhan, China, ²Laboratory for Atmospheric and Space Physics, University of Colorado Boulder, Boulder, Colorado, USA, ³Department of Atmospheric and Oceanic Sciences, University of California, Los Angeles, California, USA, ⁴Institute of Space Physics and Applied Technology, Peking University, Beijing, China

Abstract Using Van Allen Probes Relativistic Electron Proton Telescope (REPT) pitch angle resolved electron flux data from September 2012 to March 2015, we investigate in detail the global occurrence pattern of equatorial ($|\lambda| \leq 3^\circ$) butterfly distribution of outer zone relativistic electrons and its potential correlation with the solar wind dynamic pressure. The statistical results demonstrate that these butterfly distributions occur with the highest occurrence rate ~ 80% at ~ 20–04 magnetic local time (MLT) and $L > \sim 5.5$ and with the second peak (> ~ 50%) at ~ 11–15 MLT of lower L shells ~ 4.0. They can also extend to $L = 3.5$ and to other MLT intervals but with the occurrence rates predominantly < ~25%. It is further shown that outer zone relativistic electron butterfly distributions are likely to peak between 58° and 79° for $L = 4.0$ and 5.0 and between 37° and 58° for $L = 6.0$, regardless of the level of solar wind dynamic pressure. Relativistic electron butterfly distributions at $L = 4.0$ also exhibit a pronounced day-night asymmetry in response to the P_{dyn} variations. Compared to the significant L shell and MLT dependence of the global occurrence pattern, outer zone relativistic electron butterfly distributions show much less but still discernable sensitivity to P_{dyn} , geomagnetic activity level, and electron energy, the full understanding of which requires future attempts of detailed simulations that combine and differentiate underlying physical mechanisms of the geomagnetic field asymmetry and scattering by various magnetospheric waves.

1. Introduction

Electron pitch angle distributions (PADs) in the Earth's outer radiation belt are found to predominantly follow three types of appearance: the normal 90° peaked distribution, the flat-top distribution shown as approximately flat fluxes at a wide pitch angle range centered near 90° and the butterfly distribution featured by a flux minimum around 90° [e.g., Fritz et al., 2003; Gannon et al., 2007; Gu et al., 2011; Ni et al., 2015a]. As an essential characteristic of radiation belt dynamics, electron PADs and their evolution can provide important clues to investigate the physical processes responsible for radiation belt electron transport, loss, and acceleration.

From the recent Van Allen Probes MagEIS measurements of radiation belt electrons at medium energies (10s–100s keV) [Blake et al., 2013], butterfly distributions of energetic electrons with flux minima around 90° pitch angle are found to be unexpectedly persistent throughout the inner radiation belt ($L = 1.2$ –2.0) and frequently occur in the slot region ($L = 2.0$ –2.8) during geomagnetic storms [Zhao et al., 2014a]. The subsequent survey of Zhao et al. [2014b] further demonstrated that 61% of equatorial PADs of ~ 460 keV electrons can be categorized as butterfly distributions at $L = 1.5$ –3.0, thereby being the most prevalent PAD type in the inner belt and slot region.

The occurrence of butterfly distribution has been long thought as a consequence of drift shell splitting in association with magnetopause shadowing or negative gradient in radial flux profile [e.g., Sibeck et al., 1987; Selesnick and Blake, 2002]. Drift shell splitting results from the azimuthal asymmetry of the Earth's magnetic field and is significant only in the outer zone where the asymmetry is substantial, e.g., $L > \sim 5.0$ [Selesnick and Blake, 2002]. Therefore, electron butterfly distributions in the inner belt and slot region cannot be attributed to drift shell splitting or magnetopause shadowing. Some other hypotheses for 90° minimum PADs include that off-equator electrons are heated by chorus waves [e.g., Horne et al., 2003] or that radiation belt electrons are diffused by magnetosonic waves via Landau resonance [Horne et al., 2007; Mourenas et al., 2013; Xiao et al., 2015; Li et al., 2014, 2016].

In addition to electron butterfly distributions at medium energies [Zhao *et al.*, 2014a, 2014b], electron butterfly distributions also occur at relativistic energies [e.g., Xiao *et al.*, 2015], which however has not been investigated in detail yet. The purpose of this study is to statistically analyze the characteristics of butterfly distributions of outer zone ($L \geq 3.5$) relativistic electrons based on Van Allen Probes REPT data. Taken into account that the effect of drift shell splitting relates critically to the asymmetric configuration of the ambient magnetic field in association with the solar wind dynamic pressure (P_{dyn}), the variations of the occurrence characteristics of outer zone relativistic electron butterfly distribution with P_{dyn} are also investigated as a first step to explore the potential causative mechanism(s).

2. Data and Methodology

The present study uses the pitch angle resolved data sets of relativistic (≥ 1.8 MeV) electron fluxes measured by the REPT instrument onboard Van Allen Probes A and B [Baker *et al.*, 2013] for a period of 31 months from 1 September 2012 to 31 March 2015. We adopt the Level 3 REPT data sets that provide the flux values at a fixed array of 17 pitch angles.

For each time instance, we follow the criteria below to identify a butterfly PAD with 90° minimum [e.g., Zhao *et al.*, 2014a]:

1. By assigning the flux threshold value as 10^{-2} electrons/($\text{cm}^2 \text{s sr MeV}$) [Baker *et al.*, 2013] to avoid contamination from the background noise level, the number of useful points of electron flux with respect to pitch angle must be no less than 7;
2. The spacecraft location is confined within 3° of the geomagnetic equator, i.e., $|\lambda| \leq 3^\circ$, in order to ensure that nearly equatorially mirroring electrons are considered. While local pitch angles are considered in the present study, the equatorial confinement ensures that these local pitch angles are very close to their equatorial values;
3. $j(90^\circ) < \beta \times j_{avg}(90^\circ - \alpha : 90^\circ + \alpha)$, where $j(90^\circ)$ is the electron flux at 90° pitch angle, $j_{avg}(a:b)$ is the averaged electron flux over the pitch angle range between a and b , α is selected from 5° to 45° to determine the maximum value of $j_{avg}(90^\circ - \alpha : 90^\circ + \alpha)$, and β is the butterfly distribution index showing to which degree the electron PAD minimizes at 90° compared to other pitch angles. In the present study we set the threshold value of butterfly PADs as $\beta = 0.95$. The data are also checked to exclude the possibility of picking up “outflow populations” with high fluxes near the loss cone and much lower fluxes around 90° .

Some examples of electron butterfly PADs observed by Van Allen Probe A, determined based upon the above criterion, are displayed in Figure 1a for energies at 1.8 MeV and 3.4 MeV, respectively. Figure 1a (first and second columns) clearly exhibits a minimum of electron flux at 90° and the peak fluxes at pitch angles of 79° and 101° on the dayside (9–11 MLT) at $L \sim 5.2$ and at $L \sim 3.6$. Comparatively, Figure 1a (third and fourth columns) indicates that the butterfly PADs of relativistic electrons can become much more pronounced on the nightside (~ 01 MLT) at $L \sim 6.1$, which is featured by the presence of flux peak at pitch angles further away from 90° (i.e., 37° and 143°) and a large ratio between the peak flux to 90° flux. Therefore, the profile of a butterfly distribution is mainly defined by two quantities: the peak flux pitch angle and the ratio between the peak flux and 90° flux. The present investigation focuses on four REPT energies (1.8–3.4 MeV) to avoid the proximity of electron flux to the background noise level. To check the feasibility of our adoption of $\beta = 0.95$ as the threshold value of butterfly PADs, Figure 1b illustrates the ratios of $j(90^\circ)/j_{avg}$ during the longer periods (1 h) corresponding to Figure 1a. In each panel, the horizontal black line denotes the value of $\beta = 0.95$. While both the occurrence and profiles of butterfly distributions exhibit to vary largely with time, L shell, MLT, and electron energy, the individual butterfly PADs shown in Figure 1a are common during longer time intervals to justify our method to determine an electron butterfly PAD.

Based on the above criteria for electron butterfly distribution identification, we further confine our analysis to the outer radiation belt region with $L \geq 3.5$ to investigate the 31 month REPT data sets of the twin probes to establish a robust database of relativistic electron butterfly distributions. The corresponding L shell, magnetic local time (MLT), AE^* (the averaged AE value in the previous hour), and solar wind dynamic pressure (P_{dyn}) are recorded and subsequently adopted to perform a statistical analysis of the global occurrence of outer zone relativistic electron butterfly distribution and of its potential connection with AE^* and P_{dyn} .

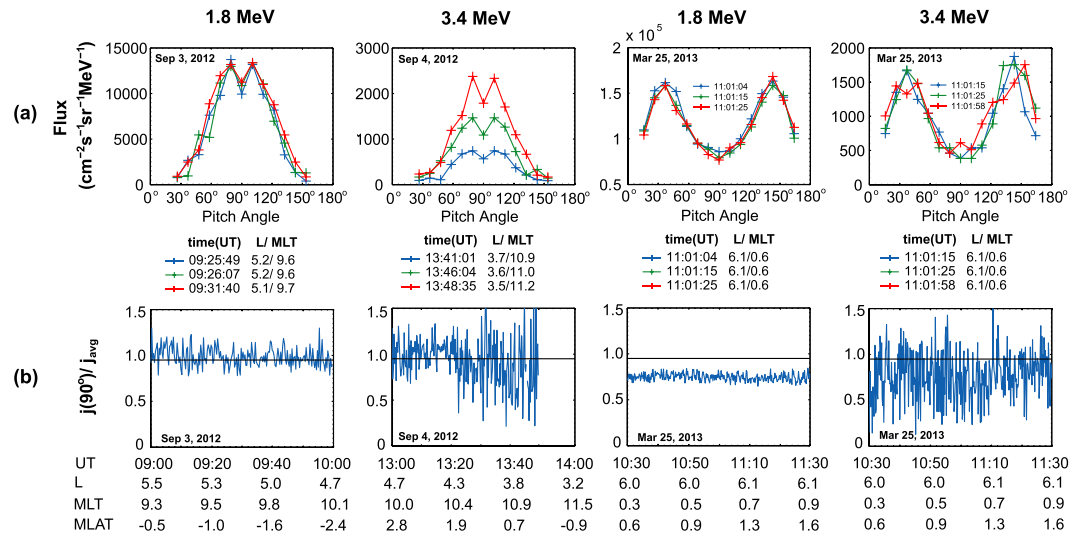


Figure 1. (a) Examples of relativistic electron butterfly pitch angle distributions observed by Van Allen Probe A for (first and third columns) 1.8 and (second and fourth columns) 3.4 MeV electrons at the specific time instances. (b) The ratios of $j(90^\circ)/j_{\text{avg}}$ during the longer periods (1 h) corresponding to Figure 1a. In each panel, the horizontal black line denotes the value of $\beta = 0.95$.

3. Global Features of Outer Zone Relativistic Electron Butterfly Distribution

Figures 2a–2d present the (L , MLT) plots of the global occurrence pattern of outer zone relativistic electron butterfly PADs for the considered four energies ((a and f) 1.8 MeV, (b and g) 2.1 MeV, (c and h) 2.6 MeV, and (d and i) 3.4 MeV) under three geomagnetic conditions ((top row) quiet, $AE^* < 100 \text{ nT}$; (middle row) moderate, $100 \text{ nT} \leq AE^* \leq 300 \text{ nT}$; and (bottom row) active, $AE^* > 300 \text{ nT}$). Figure 2e shows the number of total observation points within $|\lambda| \leq 3^\circ$ at each bin. To obtain these results, the data are binned every 0.1 L (between $L = 3.5$ – 6) times every 1 MLT h. Bins with the total points of useful pitch angle distribution below 100 are regarded as poor statistics and removed from the database (e.g., around 12 MLT for $AE^* > 300 \text{ nT}$). The occurrence rate at each bin is computed as the ratio between the number of butterfly PAD samples and the total number of observations within $|\lambda| \leq 3^\circ$. First, the butterfly PADs for relativistic electrons, as seen by Van Allen Probes, are most likely to occur on the night-to-dawnside (~ 20 – 04 MLT) at high L shells, $L > 5.5$, with a highest occurrence rate $\sim 80\%$. The second peak of the occurrence rate ($> \sim 50\%$) tends to occur at ~ 11 – 15 MLT on the dayside but at lower L shells ~ 4.0 . In addition, while exhibiting an occurrence rate typically below $\sim 25\%$, the butterfly distributions can extend to lower L shells down to $L = 3.5$ and to other MLT intervals. Second, the occurrence probability of butterfly PADs for all considered energies shows a small but discernable variation with the geomagnetic activity level. Compared to the results for quiet and moderate conditions, active time occurrence rates become larger at $L > \sim 5.5$ on the nightside with the peak shifting to the premidnight sector. Finally, while the dominant occurrence pattern is similar for the considered four REPT energies, their occurrence rates exhibit certain energy dependence. At $L = 5.0$ – 6.0 , lower energy relativistic electrons (1.8– 2.6 MeV) are much easier than 3.4 MeV electrons to evolve into a butterfly distribution.

The global distribution of bin-averaged pitch angle corresponding to outer zone relativistic electron flux peak (hereinafter defined as α_{pk}) is displayed in Figures 2f–2i in a format similar to Figures 2a–2d. There are also a number of interesting features to point out. (1) For all four energies, the smallest magnitudes of α_{pk} are constantly confined to the spatial extent of $L > \sim 4.5$ and $\text{MLT} = \sim 20$ – 05 , with the values well below 55° and down to $\sim 40^\circ$, representing the most pronounced butterfly distributions for outer zone relativistic electrons. At other MLT sectors and lower L shells, α_{pk} becomes primarily larger than 60° to manifest the butterfly distributions peaking closer to 90° . (2) As the geomagnetic activity intensifies, there is a slight trend that the butterfly distributions at $L > 4.5$ peak at lower pitch angles on the morning side but at higher pitch angles on the afternoon side, i.e., ~ 13 – 16 MLT. The butterfly PADs at $L = 3.5$ – 4.0 , while present under various geomagnetic conditions, do not show variations with the geomagnetic activity level as distinctly as those at higher L shells. (3) Overall, the characteristics of averaged peak flux pitch angle of butterfly distributions are similar for all four

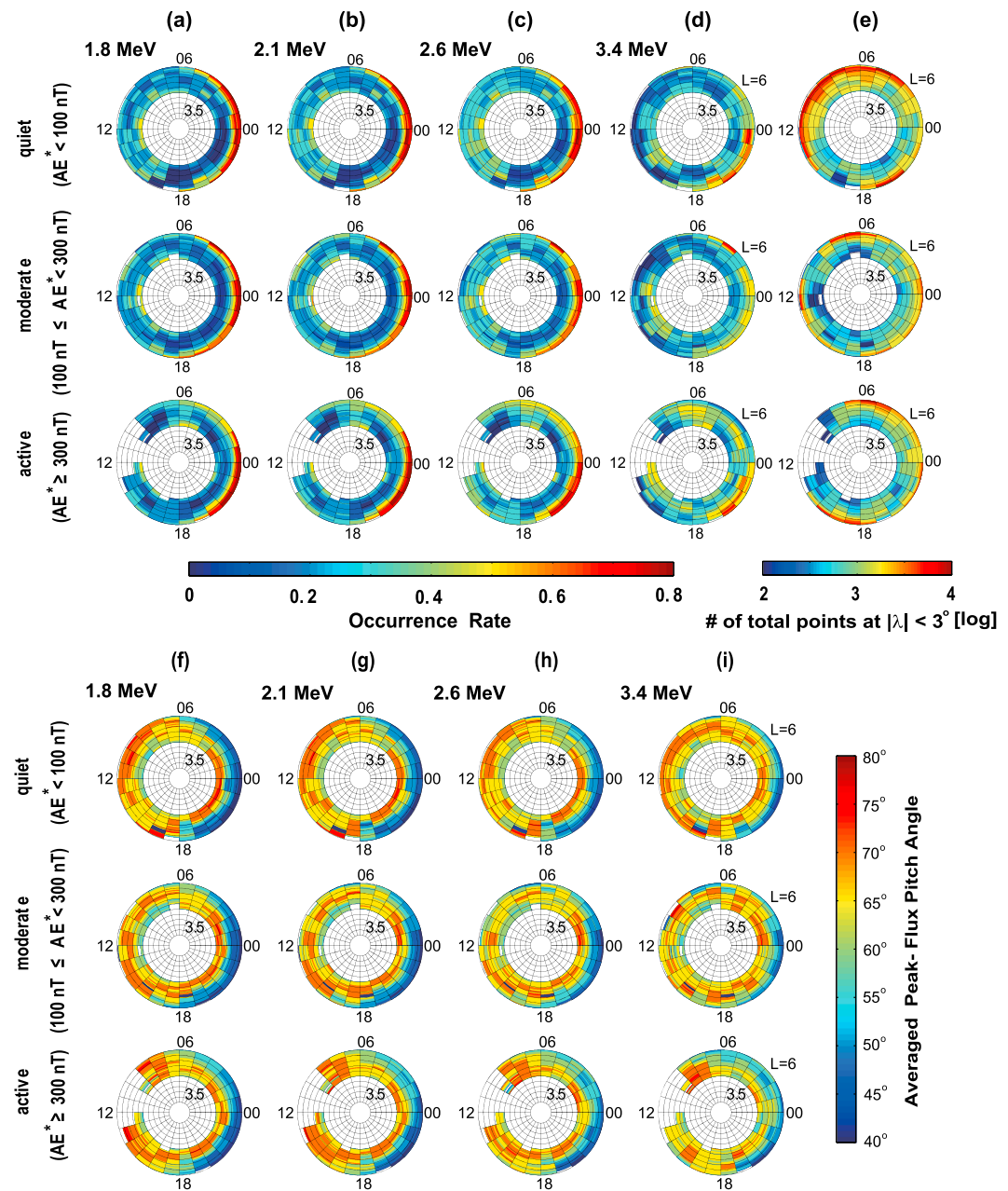


Figure 2. Global occurrence pattern of outer zone relativistic electron butterfly distribution as a function of L shell and MLT for the three levels of geomagnetic activity ((top row) quiet, (middle row) moderate, and (bottom row) active) corresponding to (a) 1.8 MeV, (b) 2.1 MeV, (c) 2.6 MeV, and (d) 3.4 MeV. (e) The corresponding numbers of total observation points at $|\lambda| \leq 3^\circ$. (f-i) The corresponding bin-averaged peak flux pitch angles (α_{pk}) for the four energies.

energies. However, in a statistical sense, the magnitudes of α_{pk} for 3.4 MeV electrons exhibit slight differences from those for lower energy electrons in that 3.4 MeV electrons tend to peak at higher pitch angles on the night-to-dawnside at $L > \sim 5.0$ and peak at lower pitch angles on the afternoon side during active periods.

4. Outer Zone Relativistic Electron Butterfly Distribution Variations With P_{dyn}

To investigate the potential connection between outer zone relativistic electron butterfly distributions and P_{dyn} , we select three specific L shells, i.e., $L = 4.0 \pm 0.1$, 5.0 ± 0.1 , and 6.0 ± 0.1 , to analyze the variation features of relativistic electron butterfly PADs with respect to P_{dyn} , the statistical results of which are shown in Figure 3.

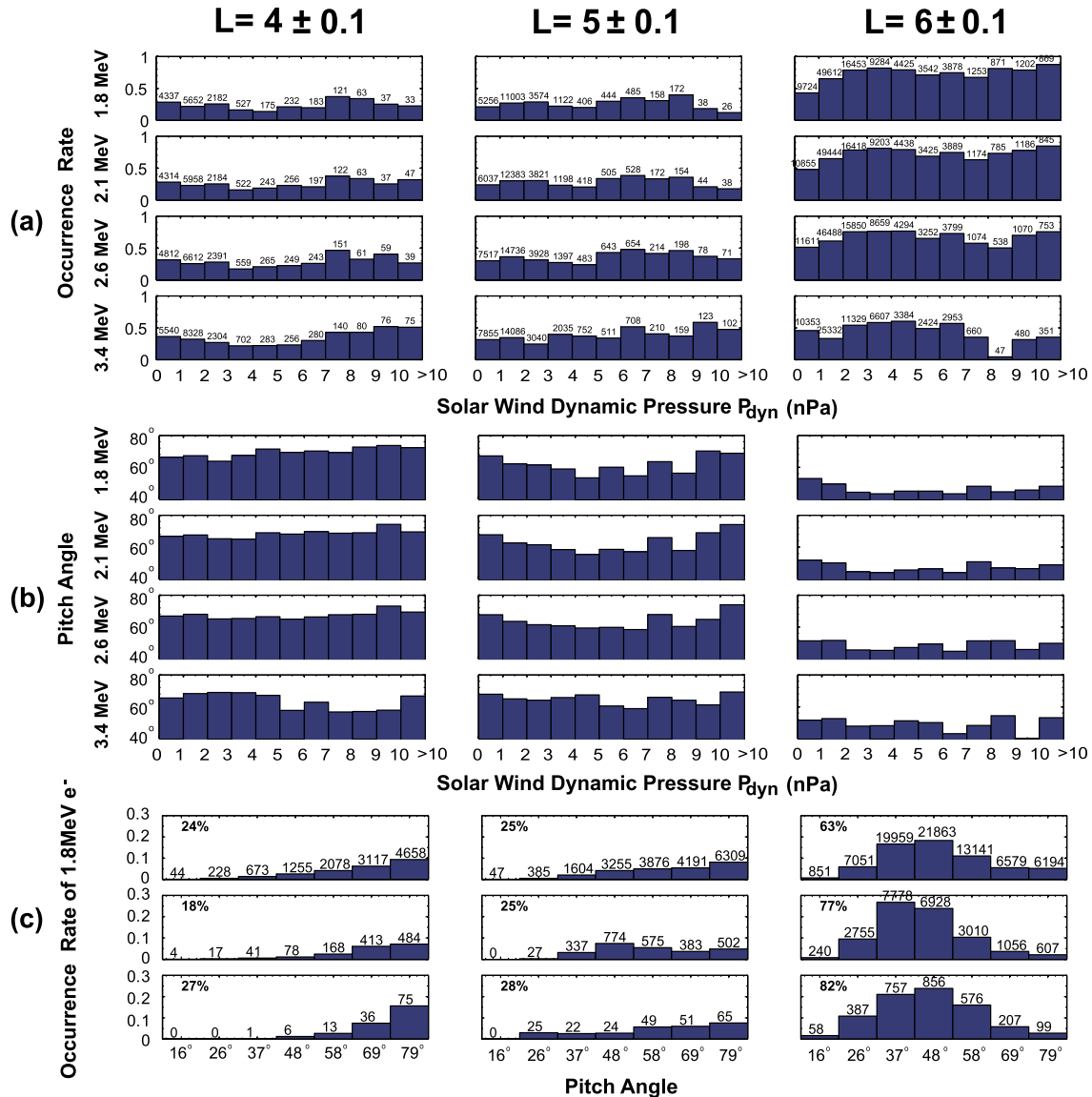


Figure 3. For the indicated three L shells, (a) histograms of the occurrence rate of butterfly PADs as a function of P_{dyn} for 1.8–3.4 MeV electrons; (b) histograms of the averaged pitch angle (α_{pk}) corresponding to the peak flux of butterfly distribution as a function of P_{dyn} for 1.8–3.4 MeV electrons; and (c) histograms of the occurrence rate of 1.8 MeV electron butterfly distributions as a function of pitch angle for the indicated three P_{dyn} levels ((top row) $P_{\text{dyn}} \leq 3$ nPa; (middle row) $3 \text{ nPa} < P_{\text{dyn}} \leq 8$ nPa; and (bottom row) $P_{\text{dyn}} > 8$ nPa).

Figure 3a displays the histograms of the occurrence rates of butterfly PADs as a function of P_{dyn} for 1.8–3.4 MeV electrons at the indicated three L shells. In each subplot are also labeled the numbers of identified butterfly PADs in each of the specified P_{dyn} interval. Similarly, the occurrence rate is computed for each specified P_{dyn} interval as the ratio between the number of butterfly PAD samples and the total number of observations within $|L| \leq 3^\circ$. Overall, the occurrence rates of outer zone relativistic electron butterfly PADs exhibit a significant dependence on L shell but an insignificant dependence on P_{dyn} and electron energy. Specifically, for 1.8–2.6 MeV electrons, the occurrence rates of butterfly PADs are largest at $L = 6.0$, varying from $\sim 50\%$ when $P_{\text{dyn}} < 1$ nPa to $\sim 90\%$ when $P_{\text{dyn}} > 10$ nPa. It is clear to see that the occurrence rates of butterfly distributions do not change much when $P_{\text{dyn}} > 2$ nPa, especially for 1.8 and 2.1 MeV electrons. At $L = 4.0$ and 5.0, the occurrence rates become much smaller, varying from $\sim 20\%$ to $\sim 50\%$ and showing a small increase when P_{dyn} increases. We see the similar trend of 3.4 MeV electrons with respect to L shell and P_{dyn} . But their occurrence rates are $\sim 30\%–60\%$ at $L = 4.0$ and 5.0 and below $\sim 65\%$ at $L = 6.0$, therefore being larger at lower L shells and smaller at higher L shells compared to the results for

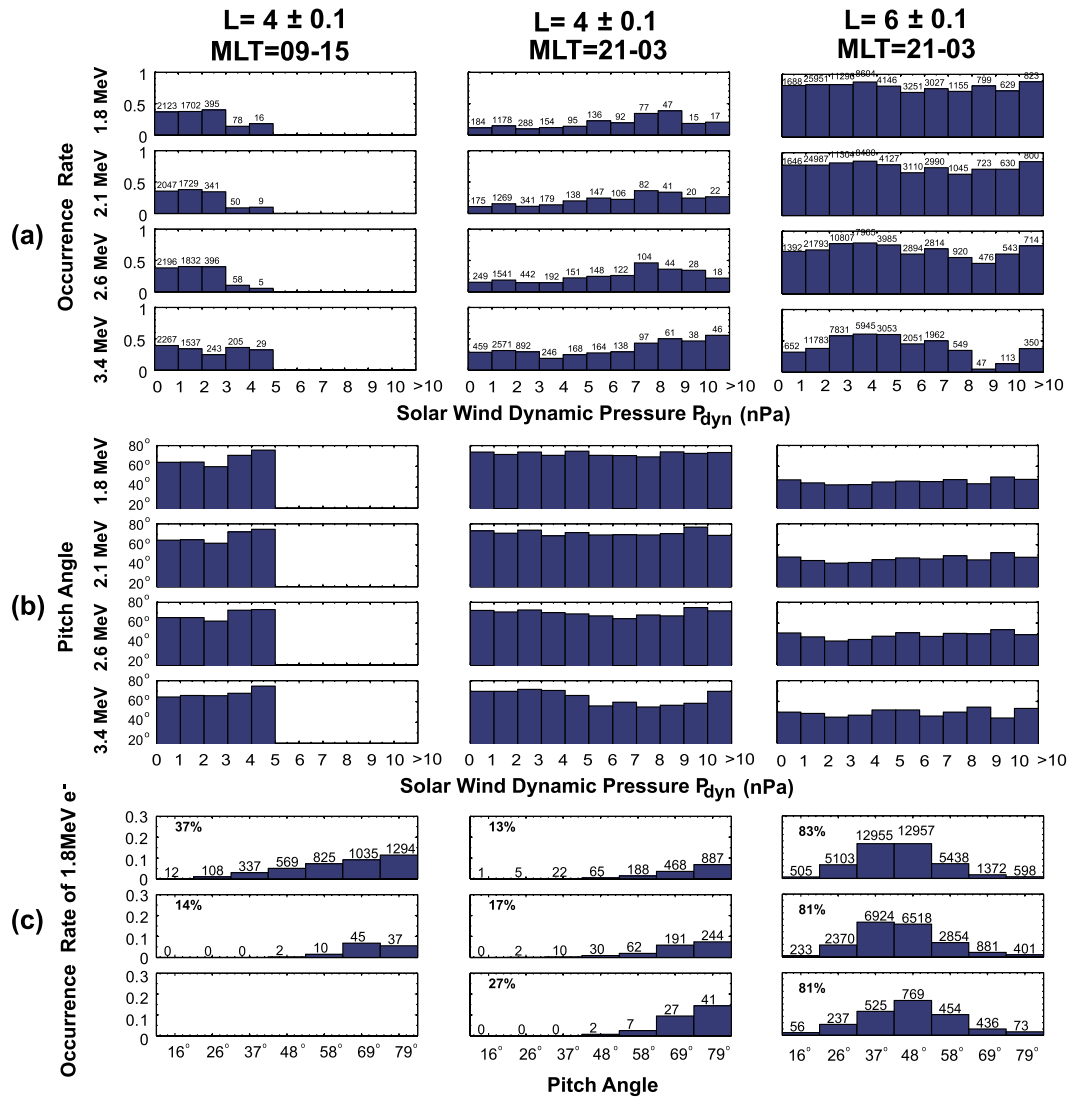


Figure 4. Similar to Figure 3, except for three specified spatial extents: (left to right columns) $L = 4.0$ on the dayside (09–15 MLT), $L = 4.0$ on the nightside (21–03 MLT), and $L = 6.0$ on the nightside (21–03 MLT).

1.8–2.6 MeV. Note that the substantially small value of the occurrence rate for 3.4 MeV electrons at $L = 6.0$ when $P_{\text{dyn}} = 8\text{--}9$ nPa is due to low counts.

Figure 3b presents the histograms of the averaged peak flux pitch angles (α_{pk}) of butterfly distributions as a function of P_{dyn} for 1.8–3.4 MeV electrons at the three L shells. The most pronounced feature is that α_{pk} is largely dependent on L shell but much less sensitive to P_{dyn} . For 1.8–2.6 MeV, α_{pk} varies between 45° and 55° at $L = 6$, between 55° and 72° at $L = 5$, and between 67° and 74° at $L = 4$, exhibiting a pronounced trend of α_{pk} decline with L shell. For 3.4 MeV electrons, the variations of α_{pk} with L shell and P_{dyn} are similar to those for lower energy electrons, but the magnitudes of α_{pk} are primarily smaller at $L = 4.0$ and larger at $L = 6.0$.

A further analysis of the occurrence features of outer zone relativistic electron butterfly PADs under various levels of P_{dyn} intensity produces Figure 3c, which illustrates the histograms of the occurrence rates of 1.8 MeV electron butterfly distributions as a function of pitch angle at $L = 4.0, 5.0$, and 6.0 (from left to right) for the indicated three P_{dyn} levels ((top row) $P_{\text{dyn}} \leq 3$ nPa, (middle row) $3 \text{ nPa} < P_{\text{dyn}} \leq 8$ nPa, and (bottom row) $P_{\text{dyn}} > 8$ nPa). On the top of each bar is also given the number of electron butterfly PADs identified at the specific peak flux pitch angle. The total occurrence rate of butterfly distributions under the specific P_{dyn} level is shown on the top left of each subplot. It is clearly seen that for 1.8 MeV electrons the total occurrence rates

of butterfly distribution show small variations with the P_{dyn} level at $L = 4.0$ and 5.0 but become increasingly P_{dyn} dependent at $L = 6.0$. The REPT peak flux pitch angle of butterfly distribution manifests a significant dependence on L shell and a small dependence on P_{dyn} . Outer zone relativistic electron butterfly PADs are most likely to peak at 58° – 79° for $L = 4.0$ and 5.0 and at 37° – 58° for $L = 6.0$. The analysis results for 2.1 – 3.4 MeV electrons are shown in the supporting information Figure S1 to exhibit variations with respect to L shell and P_{dyn} in a trend similar to 1.8 MeV electrons.

To include the MLT dependence of butterfly PADs, we focus on representative spatial extents to further evaluate the dependence of relativistic electron butterfly distributions on P_{dyn} , the results of which are displayed in Figures 4 and S2. It is shown that at $L = 4.0$ and $L = 6.0$ on the nightside (21 – 03 MLT), the characteristics of relativistic electron butterfly PADs, including the variations of both the occurrence pattern and peak flux pitch angle with P_{dyn} , are overall similar to those shown in Figure 3 without specification of MLT sector. In contrast, the features of relativistic electron butterfly PADs at $L = 4.0$ on the dayside (09 – 15 MLT) are distinctly different in response to the P_{dyn} variations, which clearly shows that the occurrence rates generally decrease with P_{dyn} and finally become zero when $P_{dyn} \geq 5$ nPa. Such a pronounced day-night asymmetry in the occurrence pattern of relativistic electron butterfly PADs at $L = 4.0$ strongly implies the correspondence to the diverse scattering effects of plasma waves in different MLT sectors, which will be further discussed in section 5. We also find that the average peak flux pitch angles are much smaller at $L = 6.0$ on the nightside than at $L = 4.0$, indicating the increased possibility of the occurrence of more pronounced relativistic electron butterfly PADs at higher L shells.

5. Discussions

Consistent with the previous studies of *Zhao et al.* [2014a, 2014b] on the occurrences of electron butterfly distribution at MagEIS energies in the inner belt and slot region, our statistical results demonstrate that butterfly distributions similarly behave as the most prevalent type of relativistic electron PAD on the night-to-dawnside at $L > \sim 5.0$. At lower occurrence rates, relativistic electron butterfly distributions also take place at other local times and L shells in the outer radiation belt.

There have been a number of physical mechanisms proposed to interpret the occurrence of radiation belt electron butterfly distribution. In contrast to the butterfly distributions occurring in the inner belt and slot region, drift shell splitting acts as an essential contributor to account for butterfly distributions occurring at higher L shells in the outer radiation belt where the azimuthal asymmetry of the geomagnetic field is significant. As a common phenomenon that the drift shells separate radially for charged particles with common guiding centers but with different pitch angles, drift shell splitting can reasonably explain the extremely high probability (e.g., $> 70\%$) of relativistic electron butterfly distributions at $L > \sim 5.0$ on the nightside (see Figures 2–4) and the similarity of the butterfly distribution occurrence pattern for all four relativistic energies [*Selesnick and Blake*, 2002]. It is worthwhile to mention that when the solar wind condition becomes highly intensified so as to push the magnetopause substantially inward, the effect of magnetopause shadowing and associated outward radial diffusion may also contribute to the occurrence of butterfly distributions at $L \sim 6.0$ near the apogee of Van Allen Probes [e.g., *Turner et al.*, 2012; *Ni et al.*, 2013a]. The small dependence of the prevalent relativistic electron butterfly PADs at $L \sim 6.0$ on the nightside on P_{dyn} (Figures 2 and 4) further suggests that in principle the P_{dyn} variation does not act as a required or significant contributor to the formation of the butterfly distribution at higher L shells. While so far we do not have a good explanation for such a small dependence on P_{dyn} , this feature reasonably agrees with the results of *Selesnick and Blake* [2002, their Figures 7–9], which demonstrated that with increasing geomagnetic activity the relativistic electron anisotropies do not change as much as is predicted, particularly on the nightside where the butterfly distributions often occur. Another possible explanation of relativistic electron butterfly PADs suggests that they can be shaped due to relativistic electron scattering in the equatorial plane of magnetic field lines that are locally deformed by currents of hot ions injected into the inner magnetosphere [*Artemyev et al.*, 2013].

However, neither drift shell splitting nor magnetopause shadowing can reasonably explain the occurrence of butterfly distributions at $L < \sim 4.0$, especially during nondisturbed periods when the ambient magnetic field is almost symmetric. The butterfly distributions at lower L shells have been proposed to be attributed to interactions with magnetospheric plasma waves. One possible mechanism for radiation belt electron butterfly distributions is the nonlocal acceleration of off-equator electrons by whistler mode chorus at higher latitudes

[e.g., Horne *et al.*, 2003], which however was not verified with either observations or simulations. This scenario is also limited to the plasma trough region, thereby raising doubts about its feasibility when the plasma-sphere is relaxed to higher L shells during quiet times. Some recent studies have proposed that magnetosonic waves, which exist both inside and outside the plasmasphere [e.g., Ma *et al.*, 2013], can efficiently produce radiation belt electron butterfly distributions through Landau resonance driven parallel acceleration [Xiao *et al.*, 2015; Li *et al.*, 2016]. There are at least two features in our statistical results tending to support the idea that magnetosonic waves should be a viable candidate causing relativistic electron butterfly distributions at lower L shells in the outer zone: the occurrences of butterfly distribution with the probability rates well above 20% on the dayside at $L < \sim 4.5$ and the energy dependence of relativistic electron butterfly distribution as well as the energy-dependent pitch angles of butterfly distribution peak fluxes. However, interactions with magnetosonic waves alone are not able to interpret all the features of relativistic electron butterfly distributions at lower L shells. For instance, magnetosonic waves are known to be sensitive to the geomagnetic activity level [e.g., Ma *et al.*, 2013], but we barely see the similar dependence of the electron butterfly distributions on the dayside. In addition, the occurrence rates of butterfly PADs at $L \sim 4.0$ tend to be very small on the nightside (Figures 2 and 4). This phenomenon, together with the day-night asymmetry of the butterfly distributions at $L = 4.0$, is possibly attributed to the involvement of various magnetospheric wave modes in relativistic electron scattering along the electron drift trajectory [see Thorne 2010, Figure 1]. These hypotheses include (1) at $L \sim 4.0$ on the dayside, dayside chorus and plasmaspheric hiss are likely to intensify with P_{dyn} or AE^* [e.g., Li *et al.*, 2011, 2015] and to cause efficient electron transport from higher to lower pitch angles [e.g., Ni *et al.*, 2013b] to inhibit the formation of butterfly PADs; (2) when relativistic electrons drift from the dayside to the nightside, electromagnetic ion cyclotron waves can also produce intense scattering loss of relativistic electrons at lower pitch angles [e.g., Kersten *et al.*, 2014; Ni *et al.*, 2015b] to weaken the butterfly distributions; (3) at $L \sim 4.0$ on the nightside, besides magnetosonic waves, other wave modes including nightside chorus (stronger than dayside chorus) and possibly plasmaspheric hiss can take place concurrently to obstruct the occurrence of relativistic electron butterfly PADs. Increased scattering effect of various plasma waves at lower L shells around the heart of the outer radiation belt, in combination with the effect of drift shell splitting, may also explain why the average peak flux pitch angles are smaller at higher L shells on the nightside than at lower L shells (Figures 2–4), the physical understanding of which is outside the scope of the present study and requires future studies.

6. Conclusions

Concerning the global occurrence pattern of equatorial ($|\lambda| \leq 3^\circ$) butterfly distribution of outer zone relativistic electrons and its underlying correlation with the geomagnetic activity level and P_{dyn} , the main conclusions are summarized as follows:

1. Outer zone relativistic electron butterfly pitch angle distributions occur with the highest occurrence rate $\sim 80\%$ on the night-to-dawnside (~ 20 – 04 MLT) at $L > \sim 5.5$ and with the second peak of the occurrence rate ($> \sim 50\%$) at ~ 11 – 15 MLT on the dayside at lower L shells ~ 4.0 . While exhibiting an occurrence rate typically below $\sim 25\%$, outer zone relativistic electron butterfly distributions can extend to lower L shells down to $L = 3.5$ and to other MLT intervals.
2. Outer zone relativistic electron butterfly distributions are most likely to peak between 58° and 79° for $L = 4.0$ and 5.0 and between 37° and 58° for $L = 6.0$. Bin-averaged peak flux pitch angles (α_{pk}) are well below 55° and down to $\sim 40^\circ$, in the spatial extent of $L > \sim 4.5$ and $MLT = \sim 20$ – 05 , to represent the most pronounced butterfly distributions. At other MLT sectors and lower L shells, α_{pk} becomes primarily larger than 60° .
3. Relativistic electron butterfly distributions at $L = 4.0$ exhibit a pronounced day-night asymmetry in response to the P_{dyn} variations, showing that the dayside (09–15 MLT) occurrence rates generally decrease with P_{dyn} and finally become zero when $P_{dyn} \geq 5$ nPa, while the nightside (21 – 03 MLT) occurrence rates manifest a trend of slight increase with P_{dyn} . The average peak flux pitch angles are much smaller at $L = 6.0$ on the nightside than at $L = 4.0$.
4. Compared to the significant L shell and MLT dependence of the global occurrence pattern, outer zone relativistic electron butterfly distributions show much smaller but still discernable sensitivity to P_{dyn} , geomagnetic activity level, and relativistic electron energy. It is also worthwhile to note that the occurrence rate of 3.4 MeV electron butterfly distributions tends to be larger at $L < \sim 4.5$ and smaller at higher L shells than those of 1.8–2.6 MeV electrons.

Acknowledgments

This work was supported by the NSFC grants 41204120, 41474141, 41304130, and 41574160 and the Projects funded by China Postdoctoral Science Foundation (2013M542051 and 2014T70732). J.B. would like to acknowledge NSF Geospace Environment Modeling grant AGS-1103064. We would like to thank Hong Zhao and Jinxing Li for their helpful discussions. We appreciate Daniel Baker, Harlan Spence, Geoffrey Reeves, and the Van Allen Probes REPT team for providing relativistic electron data. Van Allen Probes REPT data were obtained from <http://www.rbsp-ect.lanl.gov/science/DataDirectories.php>. Solar wind parameters and geomagnetic indices were obtained from the online OMNIWeb at http://omniweb.gsfc.nasa.gov/ow_min.html. We also thank the reviewers for constructive comments and valuable suggestions to improve the manuscript.

References

- Artemyev, A. V., O. V. Agapitov, F. S. Mozer, and H. Spence (2013), Butterfly pitch angle distribution of relativistic electrons in the outer radiation belt: Evidence of nonadiabatic scattering, *J. Geophys. Res. Space Physics*, **120**, 4279–4297, doi:10.1002/2014JA020865.
- Baker, D. N., et al. (2013), The Relativistic Electron-Proton Telescope (REPT) instrument on board the Radiation Belt Storm Probes (RBSP) spacecraft: Characterization of Earth's radiation belt high-energy particle populations, *Space Sci. Rev.*, **179**, 337–381, doi:10.1007/s11214-012-9950-9.
- Blake, J. B., et al. (2013), The magnetic electron ion spectrometer (MagEIS) instruments aboard the radiation belt storm probes (RBSP) spacecraft, *Space Sci. Rev.*, **179**(1–4), 383–421, doi:10.1007/s11214-013-9991-8.
- Fritz, T. A., M. Alothman, J. Bhattacharjya, D. L. Matthews, and J. Chen (2003), Butterfly pitch angle distributions observed by ISEE-1, *Planet. Space Sci.*, **51**, 205–219.
- Gannon, J. L., X. Li, and D. Heynderickx (2007), Pitch angle distribution analysis of radiation belt electrons based on Combined Release and Radiation Effects Satellite Medium Electrons A data, *J. Geophys. Res.*, **112**, A05212, doi:10.1029/2005JA011565.
- Gu, X., Z. Zhao, B. Ni, Y. Shprits, and C. Zhou (2011), Statistical analysis of pitch angle distribution of radiation belt energetic electrons near the geostationary orbit: CRRES observations, *J. Geophys. Res.*, **116**, A01208, doi:10.1029/2010JA016052.
- Horne, R. B., N. P. Meredith, R. M. Thorne, D. Heynderickx, R. H. A. Iles, and R. R. Anderson (2003), Evolution of energetic electron pitch angle distributions during storm time electron acceleration to megaelectronvolt energies, *J. Geophys. Res.*, **108**(A1), 1016, doi:10.1029/2001JA009165.
- Horne, R. B., R. M. Thorne, S. A. Glauert, N. P. Meredith, D. Pokhotelov, and O. Santolik (2007), Electron acceleration in the Van Allen radiation belts by fast magnetosonic waves, *Geophys. Res. Lett.*, **34**, L17107, doi:10.1029/2007GL030267.
- Kersten, T., R. B. Horne, S. A. Glauert, N. P. Meredith, B. J. Fraser, and R. S. Grew (2014), Electron losses from the radiation belts caused by EMIC waves, *J. Geophys. Res. Space Physics*, **119**, 8820–8837, doi:10.1002/2014JA020366.
- Li, J., et al. (2014), Interactions between magnetosonic waves and radiation belt electrons: Comparisons of quasi-linear calculations with test particle simulations, *Geophys. Res. Lett.*, **41**, 4828–4834, doi:10.1002/2014GL060461.
- Li, J., et al. (2016), Formation of energetic electron butterfly distributions by magnetosonic waves via Landau resonance, *Geophys. Res. Lett.*, **43**, 3009–3016, doi:10.1002/2016GL067853.
- Li, W., R. M. Thorne, J. Bortnik, Y. Nishimura, and V. Angelopoulos (2011), Modulation of whistler mode chorus waves: 1. Role of compressional Pc4-5 pulsations, *J. Geophys. Res.*, **116**, A06205, doi:10.1029/2010JA016312.
- Li, W., Q. Ma, R. M. Thorne, J. Bortnik, C. A. Kletzing, W. S. Kurth, G. B. Hospodarsky, and Y. Nishimura (2015), Statistical properties of plasmaspheric hiss derived from Van Allen Probes data and their effects on radiation belt electron dynamics, *J. Geophys. Res. Space Physics*, **120**, 3393–3405, doi:10.1002/2015JA021048.
- Ma, Q., W. Li, R. M. Thorne, and V. Angelopoulos (2013), Global distribution of equatorial magnetosonic waves observed by THEMIS, *Geophys. Res. Lett.*, **40**, 1895–1901, doi:10.1002/grl.50434.
- Mourenas, D., A. V. Artemyev, O. V. Agapitov, and V. Krasnoselskikh (2013), Analytical estimates of electron quasilinear diffusion by fast magnetosonic waves, *J. Geophys. Res. Space Physics*, **118**, 3096–3112, doi:10.1002/jgra.50349.
- Ni, B., Y. Y. Shprits, R. Friedel, R. M. Thorne, M. Daae, and Y. Chen (2013a), Responses of Earth's radiation belts to solar wind dynamic pressure variations in 2002 analyzed using multi-satellite data and Kalman filtering, *J. Geophys. Res. Space Physics*, **118**, 4400–4414, doi:10.1002/jgra.50437.
- Ni, B., J. Bortnik, R. M. Thorne, Q. Ma, and L. Chen (2013b), Resonant scattering and resultant pitch angle evolution of relativistic electrons by plasmaspheric hiss, *J. Geophys. Res. Space Physics*, **118**, 7740–7751, doi:10.1002/2013JA019260.
- Ni, B., et al. (2015a), Variability of the pitch angle distribution of radiation belt ultra-relativistic electrons during and following intense geomagnetic storms: Van Allen Probes observations, *J. Geophys. Res. Space Physics*, **120**, 4863–4876, doi:10.1002/2015JA021065.
- Ni, B., et al. (2015b), Resonant scattering of outer zone relativistic electrons by multiband EMIC waves and resultant electron loss time scales, *J. Geophys. Res. Space Physics*, **120**, 7357–7373, doi:10.1002/2015JA021466.
- Selesnick, R. S., and J. B. Blake (2002), Relativistic electron drift shell splitting, *J. Geophys. Res.*, **107**(A9), 1265, doi:10.1029/2001JA009179.
- Sibeck, D. G., R. W. McEntire, A. T. Y. Lui, R. E. Lopez, and S. M. Krimigis (1987), Magnetic field drift shell splitting: Cause of unusual dayside particle pitch angle distributions during storms and substorms, *J. Geophys. Res.*, **92**, 13,485–13,497, doi:10.1029/JA092iA12p13485.
- Thorne, R. M. (2010), Radiation belt dynamics: The importance of waveparticle interactions, *Geophys. Res. Lett.*, **37**, L22107, doi:10.1029/2010GL044990.
- Turner, D. L., Y. Y. Shprits, M. Hartinger, and V. Angelopoulos (2012), Explaining sudden losses of outer radiation belt electrons during geomagnetic storms, *Nat. Phys.*, **8**, 202–212, doi:10.1038/nphys2185.
- Xiao, F., C. Yang, Z. Su, Q. Zhou, Z. He, Y. He, D. N. Baker, H. E. Spence, H. O. Funsten, and J. B. Blake (2015), Wave-driven butterfly distribution of Van Allen belt relativistic electrons, *Nat. Commun.*, **6**, 8590, doi:10.1038/ncomms9590.
- Zhao, H., X. Li, J. B. Blake, J. F. Fennell, and S. G. Claudepierre (2014a), Peculiar pitch angle distribution of relativistic electrons in the inner radiation belt and slot region, *Geophys. Res. Lett.*, **41**, 2250–2257, doi:10.1002/2014GL059725.
- Zhao, H., X. Li, J. B. Blake, J. F. Fennell, S. G. Claudepierre, D. N. Baker, A. N. Jaynes, and D. M. Malaspina (2014b), Characteristics of pitch angle distributions of hundreds of keV electrons in the slot region and inner radiation belt, *J. Geophys. Res. Space Physics*, **119**, 9543–9557, doi:10.1002/2014JA020386.